Electronic Supporting Information

Electrochemical ammonia synthesis from nitrite assisted by in-situ generated hydrogen atoms on nickel phosphide catalyst

Xiao Yang,[a,d] Lei Kang,[b] Chuan-Jun Wang,[*c] Fulai Liu[a,d] and Yong Chen[*a,d]

[a] Key Laboratory of Photochemical Conversion and Optoelectronic Materials & CAS-HKU Joint Laboratory on New Materials, Technical Institute of Physics and Chemistry, Chinese Academy of Sciences, Beijing 100190, P. R. China

[b] Key Laboratory of Functional Crystals and Laser Technology, Technical Institute of Physics and Chemistry, Chinese Academy of Sciences, Beijing 100190, P. R. China

[c] College of Chemistry and Material Science, Shandong Agricultural University, Tai'an 271018, P. R. China

[d] University of Chinese Academy of Sciences, Beijing 100049, P. R. China

Author Contributions

Y. C. and C. J. W. conceptualized the study and led the project. X. Y. performed the bulk of catalyst preparation, characterization, and catalytic tests. F. L. contributed to morphology characterization. L. K. performed the theoretical calculations. All authors contributed to the writing of the manuscript and data analysis.

Experimental section

Materials. All chemicals and solvents were commercial and used as received without further purification. Ni foam (100 mm × 100 mm) was purchased from KUNSHAN JIAYISHENG ELECTRONICS CO., LTD. Carbon rod and saturated Ag/AgCl electrode was bought from Tianjin AIDA Hengsheng Science-Technology Development Co., Ltd. Nessler's reagent was bought from Chengdu HuaXia Chemical Reagent Co. Ltd. (Chengdu, China). Sodium hypophosphite (NaH2PO2, ≥99%) was obtained from Xilong Chemical CO., Ltd. (Guangdong, China). Sodium nitrite ($NaNO_2$, ≥99%) and potassium sodium tartrate ($KNaC_4H_4O_6{\cdot}4H_2O$, ≥99.7%) were bought from Beijing Beihua Fine Chemicals CO., Ltd. (Beijing, China). Sodium hydroxide (NaOH, ≥99.7%), hydrochloric acid (HCl, ≥37%) and all solvents were obtained from Sinopharm Chemical Reagent Co., Ltd. (Shanghai, China).

Preparation of Ni_2P. One piece of nickel foam (1 cm × 2 cm × 0.16 cm) were cleaned by 1 M HCl solution, ethanol and deionized water with the assistance of ultrasonication for 20 min. The pretreated Ni foam and NaH_2PO_2 (800 mg) were placed in the porcelain boat and the NaH_2PO_2 was set at the upstream side. Then the boat was put into a tube furnace, which was purged with argon (99.99%) for 20 min. The furnace was heated to 500 °C at 2 °C min^{-1}, and kept for 120 min. Finally, the furnace naturally cooled to ambient temperature. The Ar flow was maintained throughout the whole tempering process. Then the sample was taken out, washed several times by deionized water and dried in vacuum oven.

Materials Characterizations. Powder X-ray diffraction patterns (XRD) were carried out using a Bruker AXSD8. Samples for transmission electron microscopy (TEM) were analyzed by using a transmission electron microscope (JEM 2100) with an accelerating voltage of 200 kV. Scanning electron microscopy (SEM) measurements were conducted on a Hitachi SU-8100 field emission scanning electron microscope. For the TEM measurements, Ni_2P was immersed in ethanol and sonicated for at least 30 min, then dropped on an ultrathin carbon film copper mesh and allowed to dry in air at room temperature prior to these measurements. ^1H NMR experiments were performed on a 400 MHz Brucker NMR instrument with D_2O as solvent (300 μL solution and 200 μL D_2O).

Electrochemical measurements. Electrochemical measurements were performed on a computer-controlled CHI660E electrochemical workstation and conducted in a typical three-electrode setup in H-cell with Ni_2P as working electrode, carbon rod as counter electrode and a commercial Ag/AgCl as reference electrode. The experiments were conducted in an electrolyte solution of 1.0 M NaOH with 0.1 M $NaNO_2$, and stirred at a rate of 500 rpm. All the potentials reported in our work were calibrated with respect to reversible hydrogen electrode (RHE): E (RHE) = E (Ag/AgCl) + 0.197 + 0.059 pH unless stated otherwise. The theoretical potential for hydrogen evolution reaction was 0.0 V vs. RHE. The geometrical surface area of the Ni_2P electrode used for electrocatalysis is 1 cm^2 and the current density was calculated using the geometrical surface area of 1 cm2. All experiments were carried out at 25 °C without iR-correction.

The Faradaic efficiency for $NaNO_2$ reduction was defined as the quantity of electric charges used for producing ammonia divided by the total charge passing through the electrodes during the electrolysis. Six electrons are needed to produce one NH3 molecule, so the Faradaic efficiency can be calculated as follows: $FE_{NH3} = (6 \times C_{NH3} \times V \times F)/Q$, where C_{NH3} is the concentration of ammonia, V is the volume of the NaOH electrolyte, F is the Faraday constant and Q is the total number of charges passing through the catalyst.

Determination of ammonia. The quantity of NH_3 generation was determined through the colorimetric method using Nessler's reagent. First, 10 mL of the electrolyte was taken out after $NaNO_2$ reduction. Second, 0.2 mL of potassium sodium tartrate ($KNaC_4H_4O_6$, 500 g/L) was added into the solution to chelate soluble metal ion and mixed thoroughly. Third, 0.3 mL of Nessler's reagent was also added into the solution and mixed. Fourth, the solution sat for 15 min for

color development. Finally, the absorbance of the solution at 420 nm was measured using a 10 mm glass cuvette. And the concentration-absorbance curves were calibrated using standard ammonia chloride solutions, as shown in Figure S3, which contained the same concentrations of NaOH used in the electrolysis experiments.

Computational methods. The first-principles calculations are performed by the plane-wave pseudopotential method implemented in the CASTEP based on the density functional theory (DFT).S1-3 The exchange-correlation (XC) functionals is described by the local density approximation (LDA).S4 The ion-electron interactions are modeled by the ultrasoft pseudopotentialsS5 for all constituent elements. A kinetic energy cutoff of 340 eV and Monkhorst-Pack k-point meshesS6 spanning less than 0.04/Å3 in the Brillouin zone are chosen. Meanwhile, the atomic position in unit cell of compounds are fully optimized using the quasi-Newton method.S7 The convergence thresholds between optimization cycles for energy change, maximum force, maximum stress, and maximum displacement are set as 5.0×10–6 eV per atom, 0.01 eV per Å, 0.02 GPa, and 5.0×10^{-4} Å, respectively. The optimization terminates when all of these criteria are satisfied. Based on the optimized reactant and product, CASTEP transition state (TS) searches further are performed using synchronous transit methods,S8 which interpolate a reaction pathway to find a transition state and is useful for predicting barriers to chemical reactions. Complete LST/QST is adopted and begins by performing an LST (Linear Synchronous Transit)/Optimization calculation, which performs a single interpolation to a maximum energy. The TS approximation obtained in that way is used to perform a QST maximization, which alternates searches for an energy maximum with constrained minimizations in order to refine the transition state to a high degree. From that point, another conjugate gradient minimization is performed. The cycle is repeated until a stationary point is located or the number of allowed QST steps is exhausted. Then the total energies of the reactants, products and transition states are obtained to investigate the energy evolution of the catalytic path.

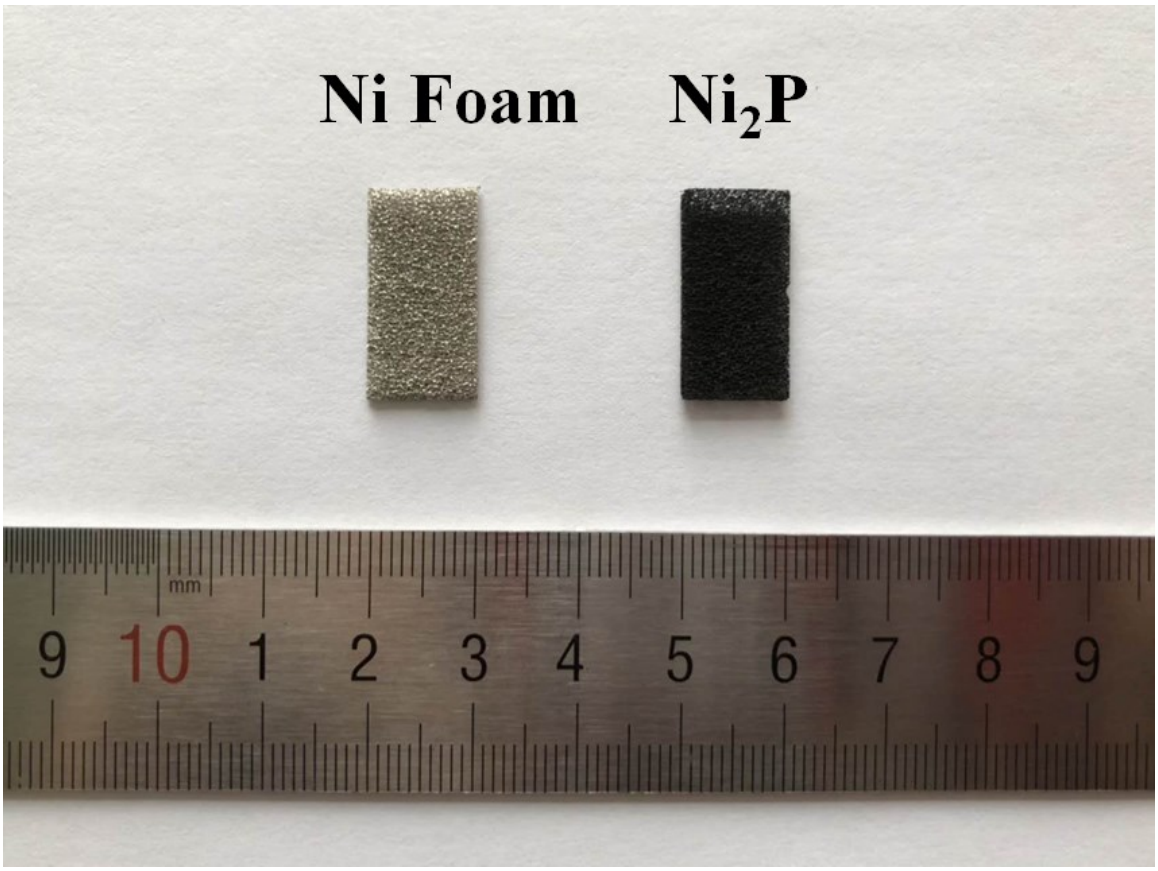

Fig. S1 Photograph of the nickel foam and Ni_2P.

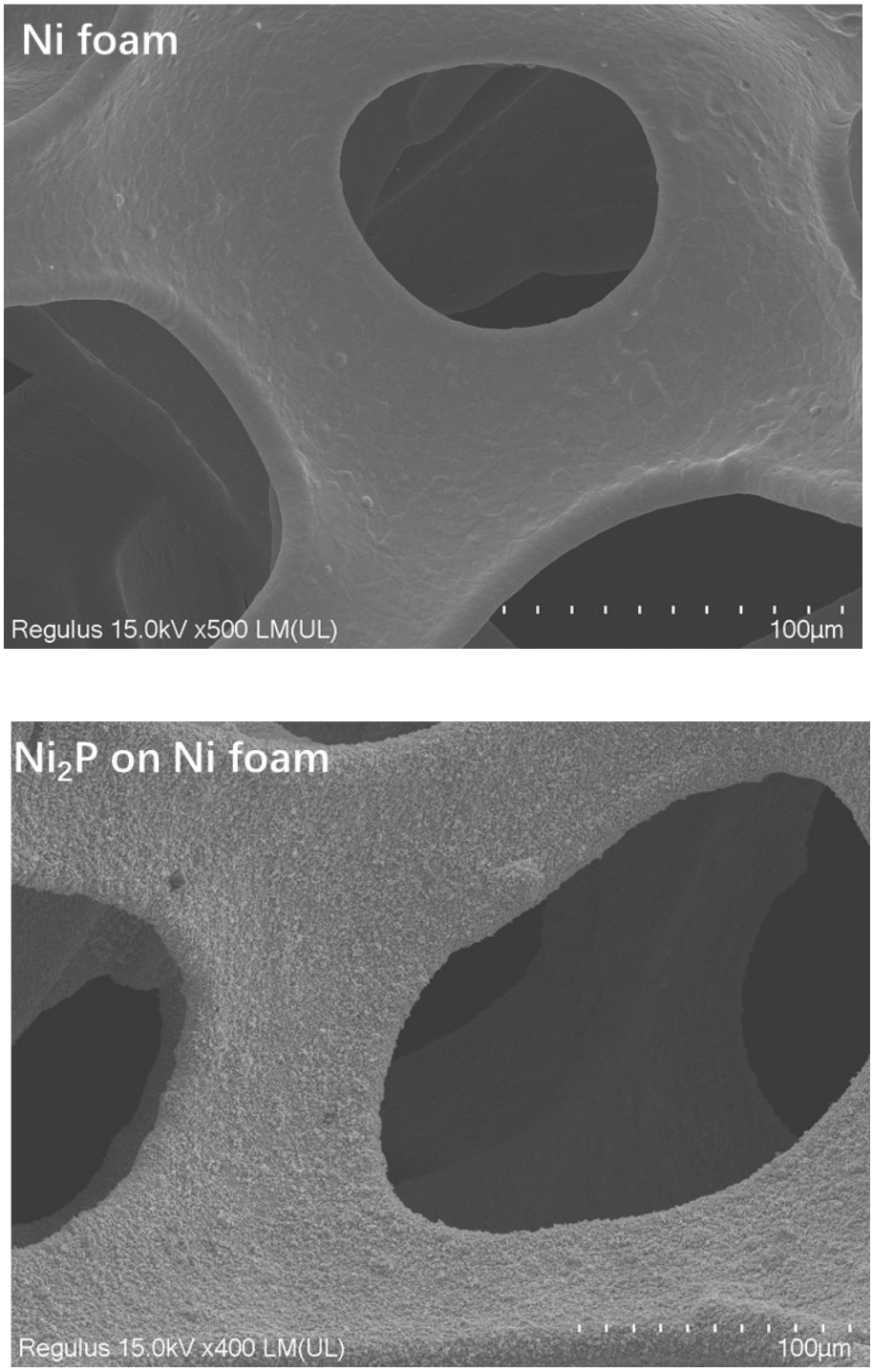

Fig. S2 SEM Photograph of the Ni foam before (Ni foam) and after phosphorization (Ni_2P on Ni foam).

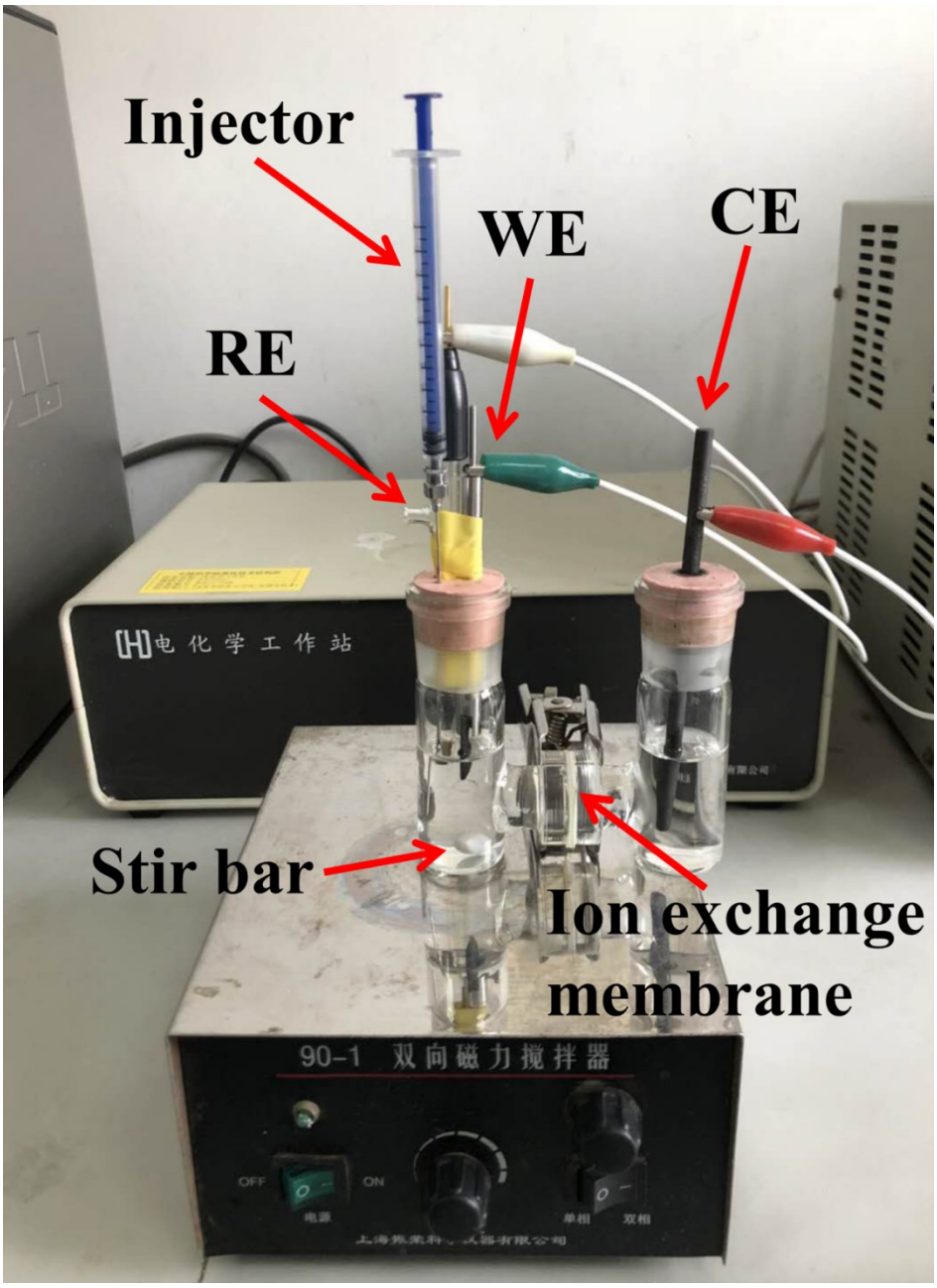

Fig. S3 Photograph of the H-cell with an injector for adding $NaNO_2$ into 1 M NaOH electrolyte.

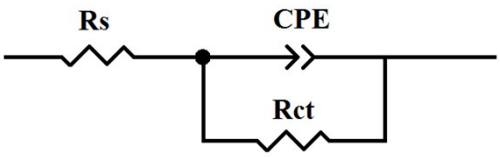

Sample	R_s (Ω)[a]	R_{ct} (Ω)[b]
Nichel Foam	1.54	48.55
Ni_2P	1.40	15.73
Nichel Foam + $NaNO_2$	1.23	9.38
Ni_2P + $NaNO_2$	1.11	0.93

[a]R_s is related to the series resistance; [b]R_{ct} denotes the charge transfer resistance.

Fig. S4 The equivalent circuit and geometric values of the electronic elements extracted from a simplified Randles equivalent circuit.

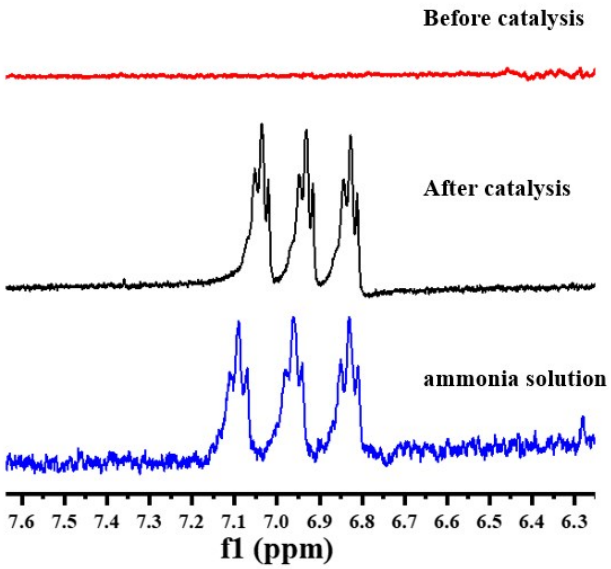

Fig. S5 ^{1}HNMR experiments performed with D_2O solvent.

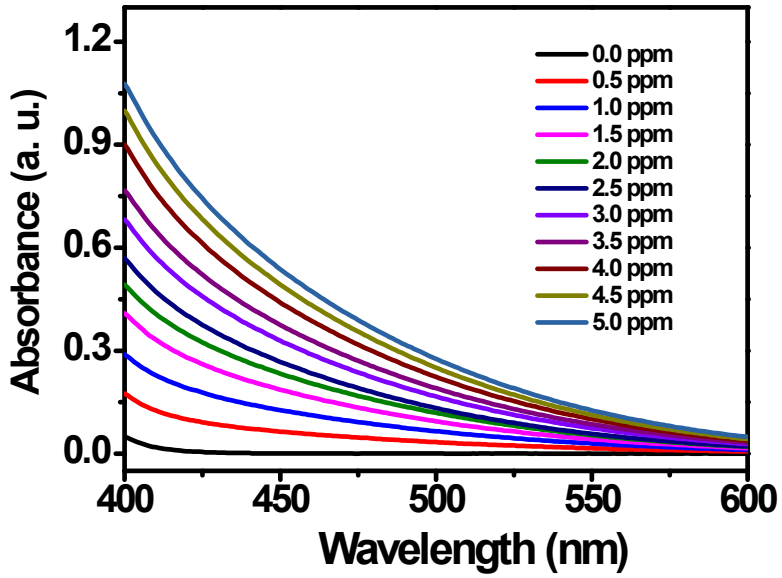

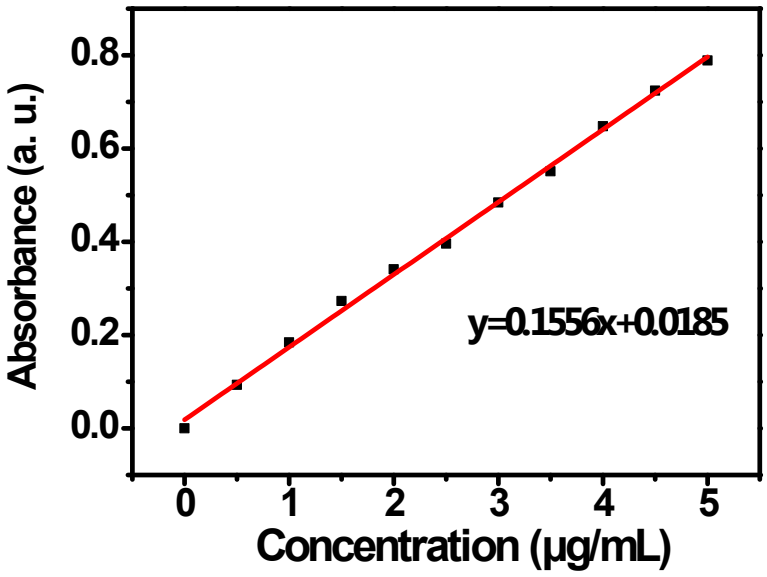

Fig. S6 Calibration curve for colorimetric NH_3 assay using Nessler's reagent.

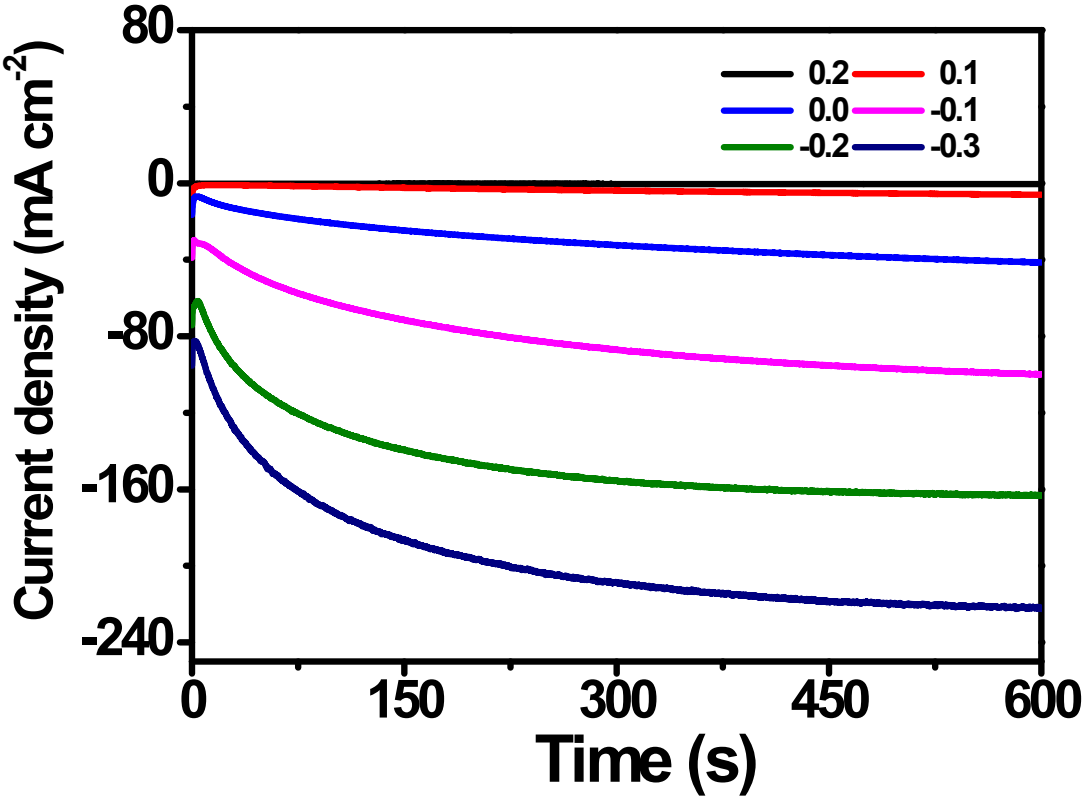

Fig. S7 Current-time plots measured at different potentials (vs. RHE) in 1.0 M NaOH with 0.1 M $NaNO_2$.

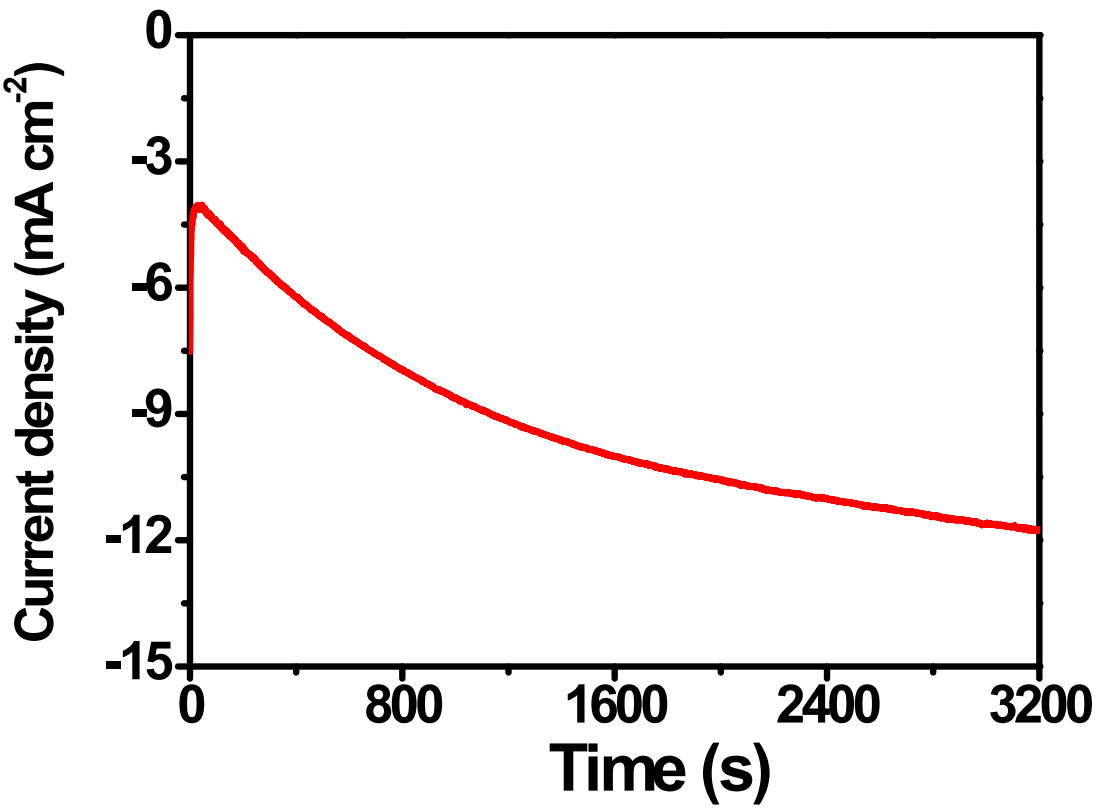

Fig. S8 Electrolysis at 0.0 V vs. RHE in 1.0 M NaOH with 0.1 M $NaNO_2$ and 0.1 M NH_3.

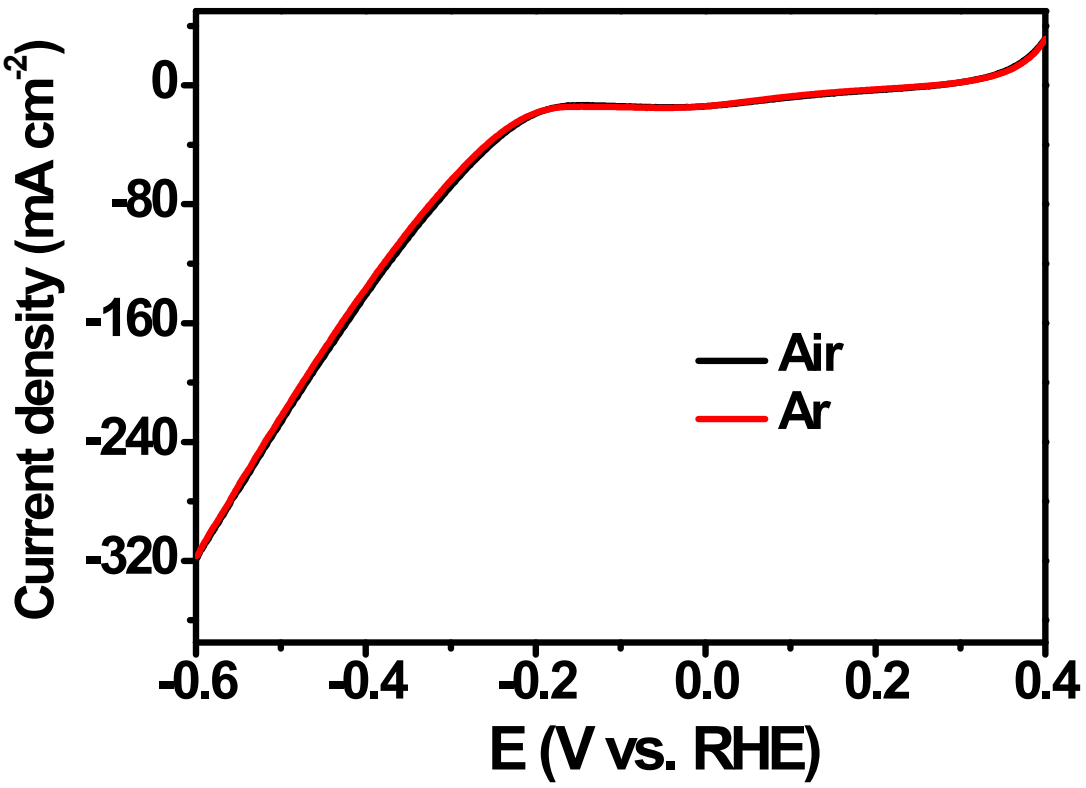

Fig. S9 LSV curves of Ni_2P saturated with Ar and air in 1 M NaOH without $NaNO_2$.

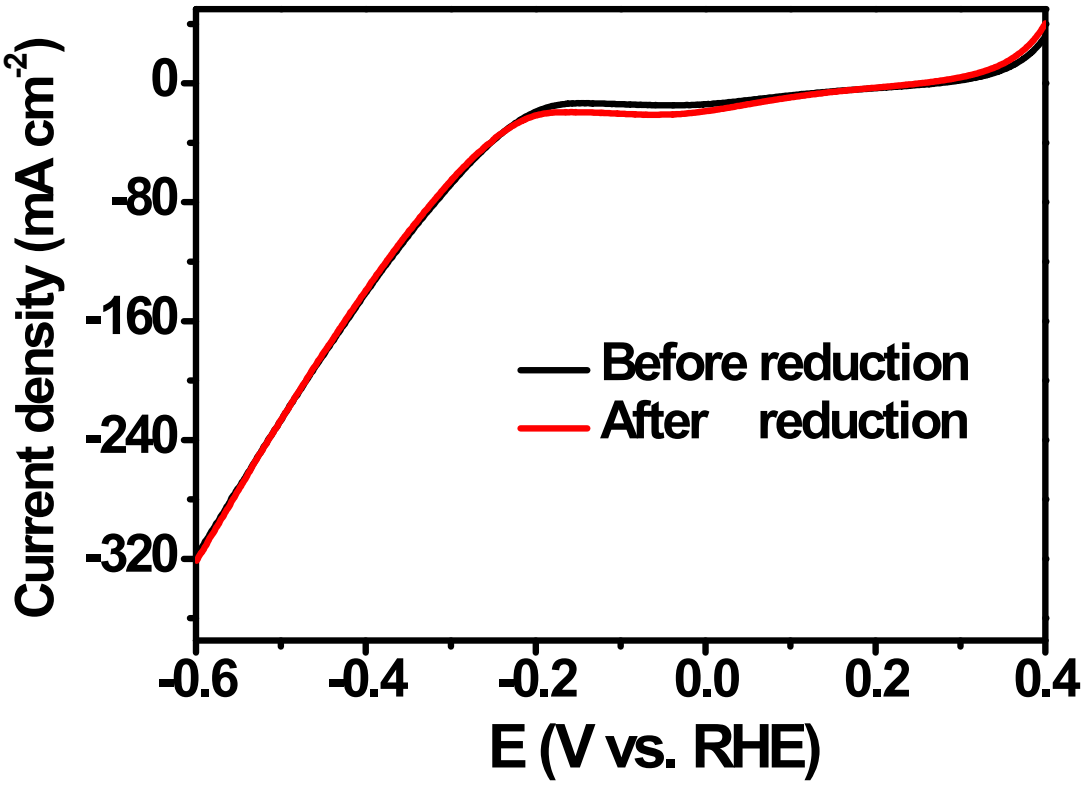

Fig. S10 LSV curves of Ni_2P before and after pre-reduction at -0.3 V vs. RHE for 200 s.

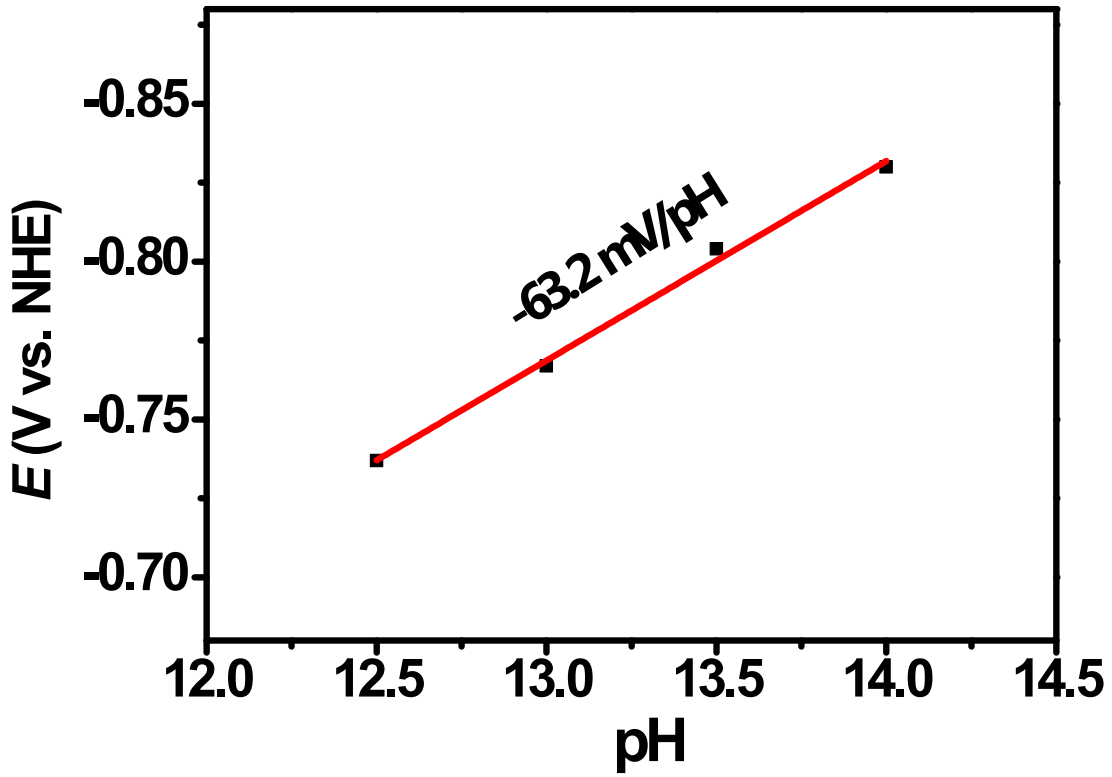

Fig. S11 Plot of potential versus pH for Ni_2P in 1 M NaOH.

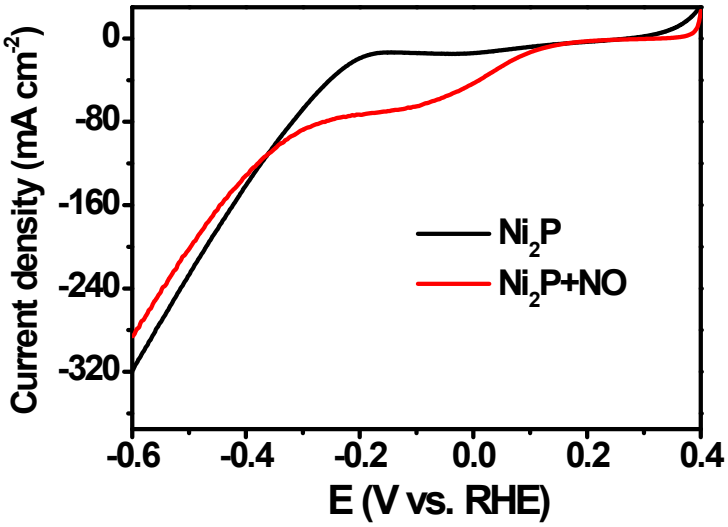

Fig. S12 LSV curves of Ni_2P in 1 M NaOH with and without NO.

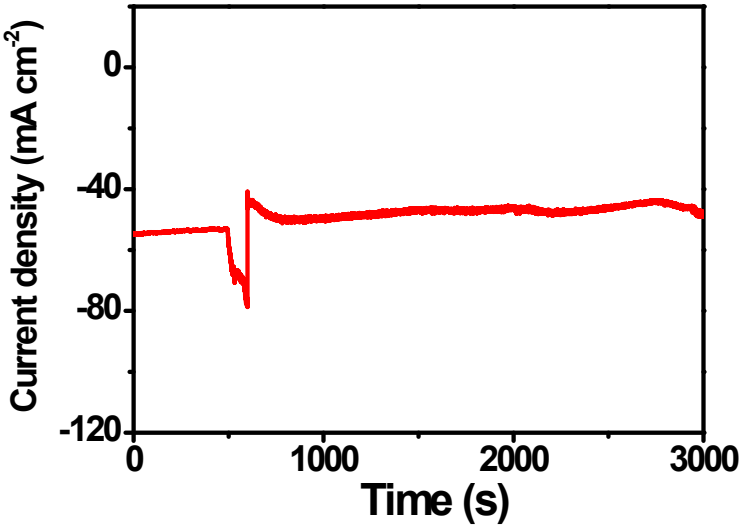

Fig. S13 HER of Ni_2P at -0.3 V vs. RHE for 500 s, followed by blowing NO into the electrolyte and changing potential to 0.0 V vs. RHE.

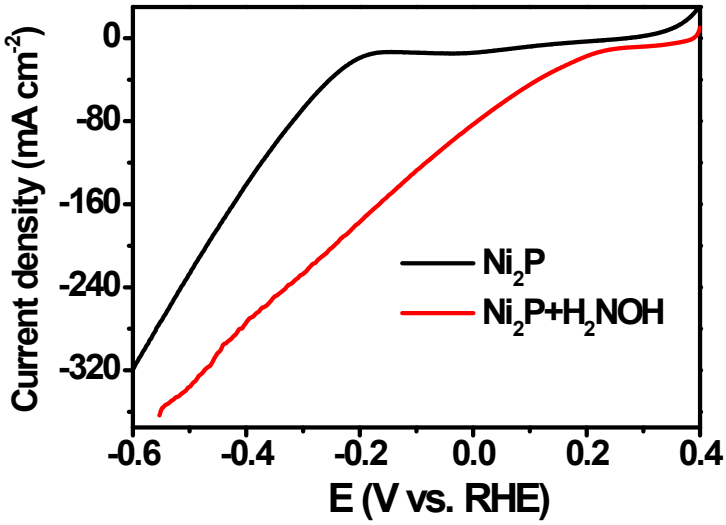

Fig. S14 LSV curves of Ni_2P in 1 M NaOH with and without 0.1 M H_2NOH.

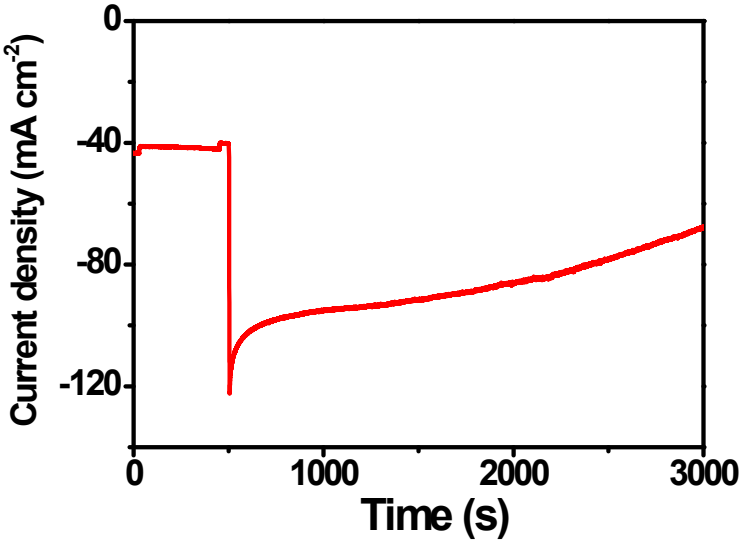

Fig. S15 HER of Ni_2P at -0.3 V vs. RHE for 500 s, followed by adding 2 mmol H_2NOH into the electrolyte and changing potential to 0.0 V vs. RHE.

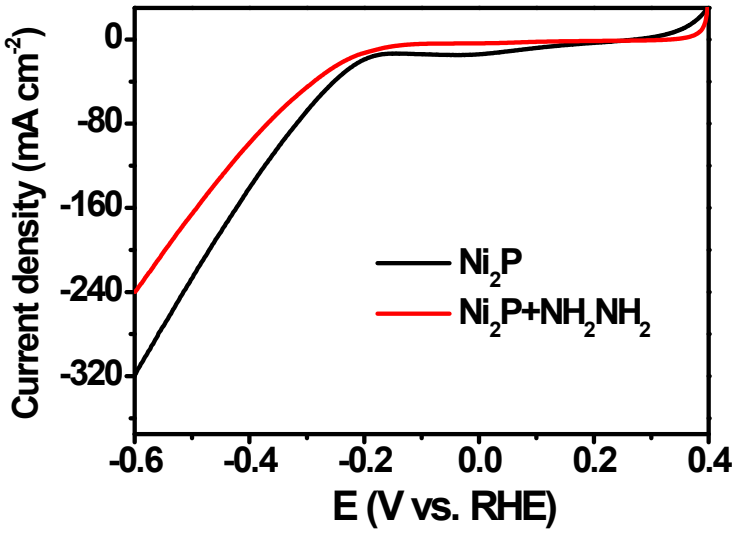

Fig. S16 LSV curves of Ni_2P in 1 M NaOH with and without 0.1 M NH_2NH_2.

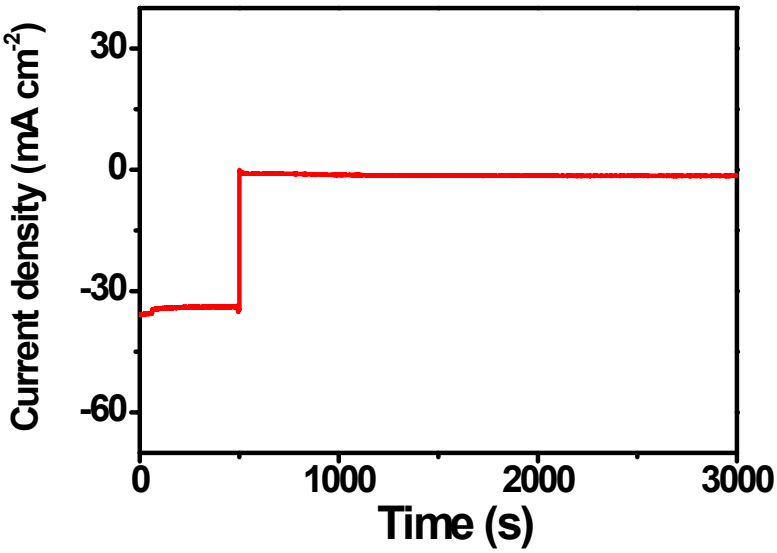

Fig. S17 HER of Ni_2P at -0.3 V vs. RHE for 500 s, followed by adding 2 mmol NH_2NH_2 into the electrolyte and changing potential to 0.0 V vs. RHE.

Table S1 Comparison of Ni_2P with the previously reported high performance nitrogen oxides reduction catalysts.

Catalysts	Conditions	Potential (V)	Ammonia synthesis rate	FE (%)	Ref.
Ni_2P	**1 M NaOH+ 0.1 M $NaNO_2$**	**0.0 *vs.* RHE**	**677.2 μmol cm^{-2} h^{-1}**	**92.6**	**This work**
$Cu_{50}Ni_{50}$	1 M KOH+ 0.1 M KNO_3	0.01 *vs.* RHE	80.7 μmol cm^{-2} h^{-1}	82.0	S9
MoFe protein	HEPES buffer (0.25 M, pH 7.4)+ 0.05 M NO_2^-	-0.57 *vs.* RHE	0.468 μmol cm^{-2} h^{-1}	~100	S10
Cu foam	0.25 M Li_2SO_4+ saturated-NO	-0.9 *vs.* RHE	517.1 μmol cm^{-2} h^{-1}	93.5	S11
Cu/Cu_2O nanowire arrays	0.5 M Na_2SO_4+ $NaNO_3$ (200 ppm of NO_3-N)	-0.85 *vs.* RHE	244.9 μmol cm^{-2} h^{-1}	95.8	10
CuPc	0.1 M KOH+ 0.1 M KNO_2	-1.3 *vs.* NHE	—	78.0	25
NiAlMnCoCu alloy	0.5 M KOH+ 0.05 M KNO_3	-0.56 *vs.* NHE	—	92.2	S12
Cobalt(II) porphyrazine	0.5 M NaOH+ 0.0028 M $NaNO_2$	-1.39 *vs.* NHE	37.1 μmol cm^{-2} h^{-1}	97.0	S13
Strained Ru nanoclusters	1 M KOH+ 1 M KNO_3	-0.2 *vs.* RHE	1170 μmol cm^{-2} h^{-1}	~100	S14
TiO_2 nanotubes with oxygen vacancies	0.5 M Na_2SO_4+ $NaNO_3$(50 ppm of NO_3-N)	-1.36 *vs.* NHE	45 μmol mg^{-1} h^{-1}	85.0	S15
Cobalt-tripeptide complex (CoGGH)	MOPS buffer (1.0 M, pH 7.2)+ 1.0 M $NaNO_2$	-0.24 *vs.* RHE	1984 μmol mg^{-1} h^{-1}	90.0	S16

FE: The Faradaic efficiency of ammonia.

References

(S1) M. C. Payne, M. P. Teter, D. C. Allan, T. A. Arias and J. D. Joannopoulos, *Rev. Mod. Phys.*, 1992, **64**, 1045-1097.

(S2) S. J. Clark, M. D. Segall, C. J. Pickard, P. J. Hasnip, M. J. Probert, K. Refson and M. C. Payne, *Z. Kristall.*, 2005, **220**, 567-570.

(S3) W. Kohn, *Rev. Mod. Phys.*, 1999, **71**, 1253-1266.

(S4) D. M. Ceperley and B. J. Alder, *Phys. Rev. Lett.*, 1980, **45**, 566-569.

(S5) J. S. Lin, A. Qteish, M. C. Payne and V. Heine, *Phys. Rev. B*, 1993, **47**, 4174-4180.

(S6) H. J. Monkhorst and J. D. Pack, *Phys. Rev. B*, 1976, **13**, 5188-5192.

(S7) B. G. Pfrommer, M. Cote, S. G. Louie and M. L. Cohen, *Journal of Computational Physics*, 1997, **131**, 233-240.

(S8) N. Govind, M. Petersen, G. Fitzgerald, D. King-Smith and J. Andzelm, *Comput. Mater. Sci.*, 2003, **28**, 250-258.

(S9) Y. Wang, A. Xu, Z. Wang, L. Huang, J. Li, F. Li, J. Wicks, M. Luo, D.-H. Nam, C.-S. Tan, Y. Ding, J. Wu, Y. Lum, C.-T. Dinh, D. Sinton, G. Zheng and E. H. Sargent, *J. Am. Chem. Soc.*, 2020, **142**, 5702-5708.

(S10) R. D. Milton, S. Abdellaoui, N. Khadka, D. R. Dean, D. Leech, L. C. Seefeldt and S. D. Minteer, *Energy Environ. Sci.*, 2016, **9**, 2550-2554.

(S11) J. Long, S. Chen, Y. Zhang, C. Guo, X. Fu, D. Deng and J. Xiao, *Angew. Chem. Int. Ed.*, 2020, **59**, 9711-9718.

(S12) C. Lu, S. Lu, W. Qiu and Q. Liu, *Electrochim. Acta*, 1999, **44**, 2193-2197.

(S13) M. Thamae and T. Nyokong, *J. Electroanal. Chem.*, 1999, **470**, 126-135.

(S14) J. Li, G. Zhan, J. Yang, F. Quan, C. Mao, Y. Liu, B. Wang, F. Lei, L. Li, A. W. M. Chan, L. Xu, Y. Shi, Y. Du, W. Hao, P. K. Wong, J. Wang, S.-X. Dou, L. Zhang and J. C. Yu, *J. Am. Chem. Soc.*, 2020, **142**, 7036-7046.

(S15) R. Jia, Y. Wang, C. Wang, Y. Ling, Y. Yu and B. Zhang, *ACS Catal.*, 2020, **10**, 3533-3540.

(S16) Y. Guo, J. R. Stroka, B. Kandemir, C. E. Dickerson and K. L. Bren, *J. Am. Chem. Soc.*, 2018, **140**, 16888-16892.